J. Fluid Mech. (1993), vol. 257, pp. 641–665

Rapid distortion analysis and direct simulation of compressible homogeneous turbulence at finite Mach number

By C. CAMBON[1], G. N. COLEMAN[2] AND N. N. MANSOUR[3]

[1] Laboratoire de Mécanique des Fluides et d'Acoustique, URA CNRS no. 263, Ecole Centrale de Lyon, 69130 Ecully, France

[2] Center for Turbulence Research, Stanford University, Stanford, CA 94305-3030, USA

[3] NASA Ames Research Center, Moffett Field, CA 94035-1000, USA

(Received 8 December 1992 and in revised form 7 May 1993)

The effect of rapid mean compression on compressible turbulence at a range of turbulent Mach numbers is investigated. Rapid distortion theory (RDT) and direct numerical simulation results for the case of axial (one-dimensional) compression are used to illustrate the existence of two distinct rapid compression regimes. These regimes – the nearly solenoidal and the 'pressure-released' – are defined by a single parameter involving the timescales of the mean distortion, the turbulence, and the speed of sound. A general RDT formulation is developed and is proposed as a means of improving turbulence models for compressible flows. In contrast to the well-documented observation that 'compressibility' (measured, for example, by the turbulent Mach number) is often associated with a decrease in the growth rate of turbulent kinetic energy, we find that under rapid distortion compressibility can produce an *amplification* of the kinetic energy growth rate. We also find that as the compressibility increases, the magnitude of the pressure–dilation correlation increases, in absolute terms, but its relative importance decreases compared to the magnitude of the kinetic energy production.

1. Introduction

This paper focuses upon the behaviour of homogeneous compressible turbulence under the influence of rapid axial (one-dimensional) mean compression. The motivation for this study is a need to cast light upon the physics of compressible turbulent flows and to improve compressible turbulence models. Our approach is to use both direct numerical simulations (DNS) and rapid distortion theory (RDT). The RDT developed in this paper is for general (those that preserve homogeneity) mean deformations; the resulting insight is then used to suggest improvements to compressible turbulence models that are applied to rapidly compressed flows.

Earlier RDT studies of homogeneous compressible turbulence have been limited to either isotropic compressions (G.A. Blaisdell 1992, private communication) or the vanishing turbulent Mach number limit (Durbin & Zeman 1992, hereafter referred to as DZ); the present investigation, therefore, attempts a more general treatment in that non-isotropic compressions and finite Mach numbers are considered. Some of our main conclusions confirm and extend those found in the recent study by Jacquin,

Cambon & Blin (1993), who use homogeneous RDT to investigate some mechanisms of shock–turbulence interactions.

An overview of our findings follows. The RDT analysis predicts that the crucial parameter for turbulence subjected to rapid compression is the ratio of the mean deformation rate, D, to the inverse sonic timescale ℓ/a, where ℓ is a turbulent lengthscale and a is the sound speed. This parameter, $D\ell/a$, hereinafter denoted as Δm (after DZ – who chose the notation since the parameter can be interpreted as the change in mean flow Mach number across an 'eddy' of size ℓ) is equivalent to the product of the inverse of the turbulent timescale, the deformation rate, and the turbulent Mach number, M_t; it defines for the dilatational part of the velocity field two distinct limits: the 'nearly solenoidal' regime given by $(\Delta m)^2 \ll 1$ (that studied by DZ) and the so-called 'pressure-released' regime with $\Delta m \gg 1$. The term 'pressure-released' (after Jacquin *et al.*) is chosen because when Δm is large, the sonic and turbulent timescales are both much larger than D^{-1} and, therefore, correlations involving the fluctuating pressure and velocity fields are negligible during a rapid distortion. The behaviour of the solenoidal velocity field, according to the RDT analysis, is unaffected by the dilatational field when the mean flow is irrotational, and is thus independent of Δm for axial compressions. Its history is, therefore, identical to that predicted for compression of purely solenoidal turbulence. In the following, we confirm these RDT predictions by comparison with DNS results.

The DNS results also show that for moderate values of Δm, all the double-velocity correlations involving the dilatational part of the turbulent velocity field remain weak with respect to the pure-solenoidal correlations and are in this sense similar to the pure solenoidal case, even for moderate compressibility (i.e. Δm). Only the $\Delta m \gg 1$ case is characterized by a strong amplification of the dilatational correlations.

The moderate-Δm results are at first glance in conflict with recent studies of axially compressed turbulence (e.g. DZ; Zeman & Coleman 1993) which find unexpectedly large pressure–dilatation correlations in the nearly solenoidal flow. This led us to investigate the behaviour of the pressure field, which has two roles for a rapid compression. On one hand, it modifies the production term in the turbulent kinetic energy equation by changing the Reynolds stress anisotropy through Π_{ij}, the classic pressure–strain rate correlation tensor (via Π_{11} for an axial compression in the x_1 direction). On the other hand, the pressure is directly involved in the kinetic energy equation through the pressure–dilatation term, $\Pi = \Pi_{ii}/2 = \overline{pu_{i,i}}/\bar{\rho}$. The magnitude of Π_{11} is found to be larger than that of Π in all cases considered in this paper for a wide range of Mach numbers and large (but finite) compression speeds.

Both the pressure variance and pressure–dilatation correlation from the DNS are found to increase with turbulent Mach number (and, therefore, with Δm at a fixed mean distortion-to-turbulent timescale ratio) *with respect to their initial values.* However, when Π is compared to *the production term* in the turbulent kinetic energy transport equation, it is much smaller and has, in fact, less relative importance with increasing M_t. This reduced relative importance of the pressure field with increasing compressibility is a key result of this paper and is the basis of much of what follows. Between the $\Delta m \to 0$ and $\Delta m \to \infty$ extremes (where for both the ratio of the pressure–dilatation correlation to the turbulent kinetic energy production is identically zero), Π must reach a maximum; from the DNS results, it appears that this maximum occurs near the $\Delta m \to 0$ limit at a small but finite value.

In the next section, the RDT analysis is developed for compressible homogeneous turbulence; in §3, the theory is applied to the case of axial compression, and separate analytic expressions for the relevant dilatational and solenoidal correlations for both

the $\Delta m \ll 1$ and $\Delta m \gg 1$ extremes are presented and compared to DNS results. The findings suggest that it would be appropriate for turbulence models to 'interpolate' between the two extremes in order to accurately capture the M_t dependence during a rapid axial compression. We propose two methods for doing so in §4, which deals with the role of, and closures for, the pressure–strain rate correlation. Section 5 considers the implications of this study for isotropically compressed and sheared flows, and §6 contains a recap of the main results and our conclusions.

2. A rapid distortion analysis for compressible homogeneous turbulence

2.1. *General considerations*

Blaisdell, Mansour & Reynolds (1991) observed that the 'intrinsic compressibility' (the non-zero divergence) of the turbulent field often tends to reduce the amplification of turbulent kinetic energy produced by a mean velocity gradient, such as a bulk compression or mean shear, with respect to the pure solenoidal case. This effect depends on at least three different timescales and on the initial turbulent field. These are the mean distortion timescale,

$$\tau_D^{-1} = (U_{i,j}U_{i,j})^{\frac{1}{2}} \tag{1}$$

(where $U_{i,j}$ is the mean velocity gradient), the 'turbulent decay' or 'turn-over' time,

$$\tau_t^{-1} = q/\ell \tag{2}$$

(where $q^2/2$ is the turbulent kinetic energy and ℓ is a lengthscale of the energy-containing eddies), and the timescale linked to the sonic speed,

$$\tau_a^{-1} = a/\ell. \tag{3}$$

The compression speed, $r = \tau_t/\tau_D$, is the only relevant parameter for modelling homogeneous incompressible turbulence (at least for large Reynolds number). However, when intrinsic compressibility is considered, the ratio of the two latter timescales, which amounts to a turbulent Mach number $M_t = \tau_a/\tau_t$, must also be accounted for. The magnitude of the reduction of the kinetic energy amplification mentioned above is, therefore, not necessarily universal, given the multi-timescale and initial-value nature of the problem. In fact, some RDT studies even go so far as to predict an *increase* with M_t of the kinetic energy amplification for turbulence under rapid (but finite) compression; these studies, by Debiève, Gouin & Gaviglio (1982) and Jacquin *et al.* (1993), are discussed in the following subsection, where the general RDT equations are presented and the reasons for the apparent growth rate versus M_t discrepancy are given. This analysis is based on an extended Craya–Herring decomposition (Cambon 1982, 1990; Cambon, Teissèdre & Jeandel 1985), which is shown to facilitate a separate investigation of the solenoidal and dilatational histories and provides a useful comparison to other approaches (e.g. Blaisdell *et al.* 1991).

Some of the earlier RDT studies have apparently over-estimated the role of the pressure–dilatation term, attempting to force an increased damping due to compressibility of the kinetic energy growth rate. We hope to clarify the situation here by separately considering various terms in one-point closure equations and thus use RDT as a tool for improving a model's representation of those terms. While the RDT is not a model in-and-of itself, by improving the accuracy of crucial terms, we expect that it will in turn also improve the overall accuracy of the model.

2.2. *Definitions and background*

To investigate the influence of the mean flow upon the turbulence, it is convenient to use a coordinate system x_i that deforms with the mean deformation. We accordingly define the Lagrangian displacement tensor F_{ij} (Eringen 1967) via

$$\mathrm{d}x_i = \frac{\partial x_i}{\partial t}\mathrm{d}t + \frac{\partial x_i}{\partial X_j}\mathrm{d}X_j = U_i\mathrm{d}t + F_{ij}\mathrm{d}X_j, \tag{4}$$

where $x_i(\boldsymbol{X}, t)$ is the position at time t of a fluid particle moving with the mean flow, which has the position X_i at the initial time $t = 0$. Representing the *substantial* time derivative by an overdot, one has

$$\dot{F}_{ij} = \frac{\partial \dot{x}_i}{\partial X_j} = \frac{\partial \dot{x}_i}{\partial x_l}\frac{\partial x_l}{\partial X_j} = U_{i,l}F_{lj} \quad \text{with} \quad F_{ij}(\boldsymbol{X}, t = 0, 0) = \delta_{ij}, \tag{5a}$$

where

$$\dot{(\ )} = (\ )_{,t} + U_j\frac{\partial(\ )}{\partial x_j} \tag{5b}$$

is the substantial derivative; where appropriate (for longer expressions) we shall also use the symbol $\mathscr{D}(\ )/\mathscr{D}t$ to denote the substantial derivative. Unless stated otherwise, the dependent variables are assumed to be decomposed into Reynolds-averaged and fluctuating components, as $U_i + u_i$, where a capital letter (and later an overbar) is used to denote Reynolds- (ensemble) averaged quantities, and lowercase (and primed, when necessary for clarity) variables denote fluctuating quantities. Note that $\boldsymbol{F}$ is a function of the stationary coordinate $\boldsymbol{X}$, the time t, and is parameterized by the time (in units of t) at which the tensor is orthonormal (hence the third argument in (5*a*)). For flows under mean compression, the determinant of $\boldsymbol{F}$ has special significance since it is equal to the volumetric ratio J.

When the mean velocity field is irrotational, the analyses proposed (over a hundred years ago!) by Cauchy, Weber, or Kelvin for the total (mean plus fluctuating) vorticity can be used to give solutions for the fluctuating vorticity ($\omega_i = \epsilon_{ijk}u_{k,j}$) and velocity fields:

$$\omega_i(\boldsymbol{X}, t) = \frac{1}{J}F_{ij}(\boldsymbol{X}, t, 0)\omega_j(\boldsymbol{X}, 0), \tag{6}$$

$$u_i(\boldsymbol{X}, t) = F_{ji}^{-1}(\boldsymbol{X}, t, 0)u_j(\boldsymbol{X}, 0) + \phi_{,i}. \tag{7}$$

These solutions, which ultimately derive from the linearized Euler equations, remain valid for inhomogeneous flows (recall the spatial dependence of $\boldsymbol{F}$) and compressible flows – provided that the baroclinic torque (in (6)) and entropy fluctuations (in (7)) are neglected; see Goldstein (1978). Equation (6) is the classic solution of the linearized Helmholtz equation when the mean vorticity–fluctuating velocity term is zero (that is, for an irrotational mean flow). When this term is not zero, simple solutions in physical space are not possible. Equation (7) (also valid only for irrotational mean flows), an expression that has been extensively used by Goldstein (1978), contains the scalar potential ϕ, which is directly connected to the fluctuating pressure ($\dot{\phi} = p/\bar{\rho}$) and can be calculated once certain assumptions are made (e.g. that the fluctuating velocity field is solenoidal or that the dilatational field is nearly acoustic). The term ϕ is not the scalar potential arising from the Helmholtz decomposition (which we will denote φ in the following) because the 'F_{ji}^{-1}' term in (7) contains contributions from both the solenoidal and dilatational velocity field.

To put the present study in context we first note that Debiève *et al.*'s (1982) RDT

solution of the Lagrangian transport equation for the Reynolds stress tensor for the case of shock wave–turbulence interaction has the form

$$\overline{u_i u_j}(t^+) = F_{mi}^{-1}(t^+, t^-)\overline{u_m u_n}(t^-)F_{nj}^{-1}(t^+, t^-), \tag{8}$$

where t^- and t^+ refer to positions upstream and downstream of the shock, respectively, following a mean streamline through the shock. The shock is considered as a pure discontinuity of the mean streamwise velocity. In other words, it is an external streamwise compression of infinite rate, and the associated tensor $\boldsymbol{F}$ does not depend on the history of the velocity gradient, but is completely characterized by the mean density jump or mean volumetric ratio $J = \mathrm{Det}(\boldsymbol{F})$, with $F_{ij} = J\delta_{i1}\delta_{j1}$ through the shock. The ratio J is linked to the upstream Mach number M_0 via

$$J = \frac{2 + (\gamma - 1)M_0^2}{(\gamma + 1)M_0^2}, \tag{9}$$

where γ is the ratio of specific heats, and use has been made of the classic Rankine–Hugoniot relations for the mean (frozen) field. A comparison of equations (7) and (8) shows that this approach *ignores* the effect of pressure (which is mediated by ϕ in (7)); the response of the pressure fluctuations with a *finite* characteristic time even for the so-called 'rapid' term is neglected compared to an *infinite* compression rate. Another idealization in the Debieve *et al.* analysis, which was also pointed out by Lee, Moin & Lele (1992), is that the distortion (curvature and unsteadiness) of the shock surface by the impinging turbulent structure is ignored. This issue, previously addressed by Ribner (1953) and Hayes (1957), is not considered in the present paper. We investigate instead the role of the pressure field in a simpler homogeneous framework by explicitly defining and formalizing the range of validity of the 'pressure released' regime that is implicit in the Debiève analysis. This paper has much in common with the recent homogeneous analysis of Jacquin *et al.* (1992), in which the pressure-released limit was first explicitly advocated.

Equation (7) shows that an irrotational deformation of a purely solenoidal velocity field is given by

$$u_i(\boldsymbol{x}, t) = u_i^s(\boldsymbol{x}, t) = \left(F_{ji}^{-1}(\boldsymbol{X}, t, 0)u_j(\boldsymbol{X}, 0)\right)^s, \tag{10}$$

where to maintain $u_{i,i} = 0$ we have,

$$\phi_{,i} = -\left(F_{ji}^{-1}(\boldsymbol{X}, t, 0)u_j(\boldsymbol{X}, 0)\right)^d \tag{11}$$

(where the s and d superscripts (and later subscripts) are understood to respectively refer to the solenoidal and dilatational contributions). The latter equation for the potential ϕ is easily rewritten as a Poisson equation,

$$\nabla^2\phi = -\left(F_{ji}^{-1}u_j\right)_{,i}, \tag{12}$$

which is a time-integral form of the classic Poisson equation for the fluctuating pressure. For the solenoidal case, the pressure 'kills off' the dilatational contribution, resulting in the lower limit of the kinetic energy growth rate caused by the mean compression. Conversely, in the pressure-released regime, the u_i^d contribution in (11) is no longer 'removed' by the pressure, producing an extra contribution to the solenoidal energy, which is unaffected by the dilatation field and again grows in accordance with (10); in other words, the compressibility leads to an increase in the kinetic energy growth rate.

From this point hence, the RDT analysis will be continued under the assumption of flow homogeneity and use made of a spectral formalism; the Fourier wave-space

proves to be invaluable for obtaining tractable RDT solutions. Beginning with (6), we shall use the Fourier space to extract the solenoidal velocity from the vorticity, as was done by Batchelor & Proudman (1954). Instead of solving a Poisson equation in physical space, we use a simple geometric wave-space projection to invoke the Helmholtz decomposition.

2.3. *The mean flow*

Before turning to the turbulent fields, however, we determine the types of mean deformations that are admitted by this analysis – i.e. those that preserve the homogeneity of the flow. In incompressible turbulence, the constraint of maintaining homogeneous statistical properties leads to two conditions: the mean velocity gradient $U_{i,j}$ must be uniform in space, and the mean flow must be a particular solution of the Navier–Stokes equations. The last condition amounts to an irrotational mean acceleration, so that

$$\nabla \times \Gamma = \mathbf{0}, \tag{13}$$

or that

$$\dot{U}_{i,j} + U_{i,l}U_{l,j}$$

is symmetric, where

$$\Gamma_i = (\dot{U}_{i,j} + U_{i,l}U_{l,j})x_j = \ddot{F}_{ij}(t,0)X_j. \tag{14}$$

Compressibility introduces a new condition. The linearization of the momentum equation displays two acceleration terms. The first one is the product of mean density and the fluctuating acceleration and leads to the same constraint mentioned above. The second term is the product of density fluctuation ρ' by the mean acceleration Γ and is typically non-homogeneous (as can be seen by the spatial dependence in (14)). This term can be removed, and homogeneity preserved, by neglecting the density fluctuation with respect to the mean density. Such an approximation (which is consistent with 'compressed' turbulence at low Mach number) will be not used in this paper. Instead, we admit only mean flows without convective acceleration. From (5) and (14) we see that this requires

$$F_{ij}(t,0) = \delta_{ij} + A_{ij}t, \tag{15a}$$

or

$$U_{i,j}(t) = A_{il}F_{lj}^{-1} = A_{il}\left(\delta_{lj} + A_{lj}t\right)^{-1}. \tag{15b}$$

Equation (15) is valid for an arbitrary constant (not necessarily symmetric) matrix $\boldsymbol{A}$ for arbitrary times, provided that the determinant of $\boldsymbol{F}$, J, remains positive. Special cases of (15) have been given previously, for example, for pure strain and shear (Blaisdell *et al.* 1991). A good approximation for the mean pressure P as a function of J can be derived from the isentropic relations. (While the isentropic relations are not strictly valid when M_t is non-zero, DNS of finite-M_t turbulence under mean compression have shown that the deviation from the isentropic prediction is relatively small: for example, in the rapid axial compression case with initial $M_t = 0.29$ discussed below, the mean pressure is within 6% of the isentropic value after a five-fold density increase.)

2.4. *The fluctuating flow*

The linearized Euler equations (with $\rho' \Gamma_i = 0$) in the deforming coordinate system are

$$\dot{u}_i + U_{i,j} u_j = -\frac{p_{,i}}{\overline{\rho}} \tag{16}$$

with $\overline{\rho} = \overline{\rho}(t) = \overline{\rho}(0)/J(t)$ (recall that the dot superscript denotes a *substantial* derivative). The linearized equations for the fluctuating pressure p and entropy s read (see DZ)

$$\left(\frac{\dot{p}}{\gamma P}\right) = -u_{i,i}, \qquad \dot{s} = 0, \tag{17}$$

where $P = \overline{\rho} R \overline{T}$. An investigation of the coupling between solenoidal and dilatational contributions to the fluctuating velocity field is conveniently done by transforming the variables in (the deformed coordinate) $\boldsymbol{x}$ into (three-dimensional) Fourier space, which we indicate either by a caret symbol or the notation '$\widehat{\mathscr{F}}(\ )$'. The classic Helmholtz decomposition is given first in physical and then in spectral space as follows:

$$v_i(\boldsymbol{X}, t) = \epsilon_{ijl} \psi_{l,j} + \varphi_{,i}, \tag{18}$$

$$\hat{v}_i(\boldsymbol{k}, t) = \left(\delta_{ij} - \frac{k_i k_j}{k^2}\right) \hat{v}_j + \frac{k_i k_j}{k^2} \hat{v}_j, \tag{19}$$

for any vector field $\boldsymbol{v}$. The two terms on the right-hand sides correspond to $\boldsymbol{v}^s$ and $\boldsymbol{v}^d$, which are defined in physical space by the vector ψ_i and the scalar potential φ. The corresponding spectral space decomposition into $\hat{\boldsymbol{v}}^s$ and $\hat{\boldsymbol{v}}^d$ is given by the projection operators in (19), which separate the (single-component) dilatational contribution parallel to the wavevector $\boldsymbol{k}$ from the (two-component) solenoidal contribution in the plane normal to $\boldsymbol{k}$. Equations (16) and (17) are easily Fourier-transformed; only the advection term requires particular caution:

$$\hat{u}_i = \widehat{\mathscr{F}}\left(u_{i,t} + U_{j,l} x_l u_{i,j}\right),$$

so

$$\hat{u}_i = \hat{u}_{i,t} - U_{l,l} \hat{u}_i - U_{j,l} k_j \frac{\partial \hat{u}_i}{\partial k_l}.$$

The first and the last terms in the right-hand side of the latter equation are collectively treated as a derivative along characteristic curves, which plays the same role as the mean trajectories in physical space. This derivative will, therefore, also be represented by an overdot so that

$$\dot{k}_i + U_{j,i} k_j = 0, \quad \text{with solution} \quad k_i = F_{ji}^{-1}(t, 0) K_j. \tag{20}$$

The analogy with physical space is complete, since

$$\dot{x}_i - U_{i,j} x_j = 0, \quad \text{with solution} \quad x_i = F_{ij}(t, 0) X_j. \tag{21}$$

The initial $\boldsymbol{k}$ value, $\boldsymbol{K}$, plays the same role in wave space as the Lagrangian coordinate $\boldsymbol{X}$ does in physical space. Pure kinematic distortion by advection in physical and spectral space are linked by a wave conservation law

$$\exp(\mathrm{i} k_j x_j) = \exp(\mathrm{i} K_j X_j),$$

where $\mathrm{i}^2 = -1$. Accordingly, one has

$$\widehat{\mathscr{F}}(\dot{u}_i) = \dot{\hat{u}}_i - U_{l,l} \hat{u}_i, \tag{22}$$

and equation (16) becomes

$$\dot{\hat{u}}_i - U_{l,l}\hat{u}_i + U_{i,j}\hat{u}_j = -\mathrm{i}k_i\frac{\hat{p}}{\rho}. \tag{23}$$

In the latter equation, the projection operators in (19) can be used to separate solenoidal and dilatational contributions. We prefer to use a slightly different method by specifying a special frame for the solenoidal mode, according to an extended Craya–Herring decomposition (Cambon 1990). An orthonormal frame of reference $(\boldsymbol{e}^{(1)}, \boldsymbol{e}^{(2)}, \boldsymbol{e}^{(3)})$ attached to the wavevector is used with the last vector being parallel to $\boldsymbol{k}$ ($e_i^{(3)} = k_i/k$, where k is the wavevector modulus). In this local frame, the Fourier transform of the velocity fluctuation reads

$$\hat{u}_i(\boldsymbol{k}, t) = \hat{\varphi}^{(1)}(\boldsymbol{k}, t)e_i^{(1)}(\boldsymbol{k}) + \hat{\varphi}^{(2)}(\boldsymbol{k}, t)e_i^{(2)}(\boldsymbol{k}) + \hat{\varphi}^{(3)}(\boldsymbol{k}, t)e_i^{(3)}(\boldsymbol{k}). \tag{24}$$

The two first terms give exactly $\hat{u}_i^s$, and the latter gives $\hat{u}_i^d$, with a minimal number of components and conservation of all the tensorial properties (invariants) due to the orthonormal properties of the local frame. Classic descriptions in terms of vorticity and divergence are easily recovered as

$$\hat{\omega}_i = \mathrm{i}k(\hat{\varphi}^{(1)}e_i^{(2)} - \hat{\varphi}^{(2)}e_i^{(1)}) \tag{25a}$$

and

$$\hat{d} \equiv \hat{u}_{i,i} = \mathrm{i}k\hat{\varphi}^{(3)}. \tag{25b}$$

In order to remove the uncertainty regarding the azimuthal position of the solenoidal coordinates with respect to $\boldsymbol{e}^{(3)}$, the $(\boldsymbol{e}^{(1)}, \boldsymbol{e}^{(2)})$-plane is defined by choosing a fixed spherical-coordinate polar axis $\boldsymbol{n}$, after Herring (1974). (Craya 1958 implicitly used $n_i = \delta_{i3}$ and addressed only covariance matrices of the velocity field and thus limited the generality of his approach.) We set

$$\boldsymbol{e}^{(1)} = \frac{\boldsymbol{k} \times \boldsymbol{n}}{|\boldsymbol{k} \times \boldsymbol{n}|} \quad \text{and} \quad \boldsymbol{e}^{(2)} = \boldsymbol{e}^{(3)} \times \boldsymbol{e}^{(1)}. \tag{26}$$

Striking simplifications can be made by choosing the polar axis according to the symmetries of the mean flow (if any) or the statistical properties of the fluctuating field, retaining the full generality of the method. The equations in the local frame can be made nearly independent of the choice of $\boldsymbol{n}$ by using the 'helical modes' $(e_i^{(2)} - \mathrm{i}e_i^{(1)}, e_i^{(2)} + \mathrm{i}e_i^{(2)})$ (which are also eigenmodes of the plane rotation matrix around $\boldsymbol{k}$ and of the 'curl' operator) as the basis set (see Greenspan 1968; Cambon & Jacquin 1989; Waleffe 1993). Substituting (24) into (23) leads to the linear system of equations for the three components of $\hat{u}_i$ in the local Craya–Herring frame, with

$$\dot{\hat{\varphi}}^{(\alpha)} - U_{l,l}\hat{\varphi}^{(\alpha)} + m_{\alpha\beta}\hat{\varphi}^{(\beta)} + m_{\alpha 3}\hat{\varphi}^{(3)} = 0, \tag{27}$$

$$\dot{\hat{\varphi}}^{(3)} - U_{l,l}\hat{\varphi}^{(3)} + m_{33}\hat{\varphi}^{(3)} + m_{3\alpha}\hat{\varphi}^{(\alpha)} + \mathrm{i}k\frac{\hat{p}}{\rho} = 0. \tag{28}$$

Greek indices (indicating solenoidal space) take only the value 1 or 2, whereas the Latin indices range from 1 to 3 (and the Einstein summation convention is assumed). Calculation of the matrix m_{ij} is straightforward; remembering to account for the time derivative of $\boldsymbol{e}^{(i)}$ with fixed $\boldsymbol{K}$, using (20) and (26), the elements are

$$m_{\alpha\beta} = e_i^{(\alpha)}U_{i,j}e_j^{(\beta)} - \dot{e}_i^{(\alpha)}e_i^{(\beta)} = e_i^{(\alpha)}U_{i,j}e_j^{(\beta)} - \epsilon_{\alpha\beta 3}R_E, \tag{29a}$$

$$m_{\alpha 3} = e_i^{(\alpha)}U_{i,j}e_j^{(3)} - \dot{e}_i^{(\alpha)}e_i^{(3)} = e_i^{(\alpha)}(U_{i,j} - U_{j,i})e_j^{(3)}, \tag{29b}$$

$$m_{3\alpha} = e_i^{(3)} U_{i,j} e_j^{(\alpha)} - \dot{e}_i^{(3)} e_i^{(\alpha)} = 2 e_i^{(3)} U_{i,j} e_j^{(\alpha)}, \tag{29c}$$

$$m_{33} = e_i^{(3)} U_{i,j} e_j^{(3)}. \tag{29d}$$

The rotation term R_E is $e_i^{(2)} U_{i,j} e_j^{(1)}$ if the polar axis is chosen as one of the eigenvectors of the mean gradient matrix; its general expression is available in Cambon *et al.* (1985). The last equation relevant to our study is that which governs the pressure:

$$\left(\frac{\dot{\hat{p}}}{\gamma P}\right) - U_{l,l}\left(\frac{\hat{p}}{\gamma P}\right) = -\hat{d} = -\mathrm{i}k\hat{\varphi}^{(3)}. \tag{30}$$

Without mean distortion, (28) and (30) correspond to a pure acoustic regime, where energy is exchanged between dilatational velocity and pressure at a frequency ak. (The sonic speed a is easily reintroduced using the isentropic relation $a^2 = \gamma R\overline{T} = \gamma\overline{p}/\overline{\rho}$.) On the other hand, the (exact) balance between the two last terms in (28) is the equivalent in physical space of the Poisson equation for p in the pure solenoidal flow. The solenoidal contribution to velocity is seen to be completely uncoupled from the dilatational field if $m_{\alpha 3}$ is zero. This is valid for *any* irrotational compressing mean flow, *but not for pure shear*, as has been stressed by Blaisdell *et al.* (1991). (The shear case is discussed further in §5). Finally, we note that the coupling of the solenoidal and dilatational fields is mediated by $m_{3\alpha}$. This term is zero for spherical compression but must be considered for any anisotropic straining process (except for very specific wavevectors given by the particular deformation). An investigation of the timescales in (28) introduces the parameter $R_a(k) \equiv (\tau_D)^{-1}/ak$, for which Δm is an averaged approximation in physical space. For very low values of this parameter, the incompressible limit is recovered, the dilatational mode $\varphi^{(3)}$ tends to zero, and the sonic speed a approaches infinity; both $k\hat{p}/\overline{\rho}$ (which tends to the solenoidal solution of the Poisson equation) and its time derivative (which from (30) is observed to be proportional to $a^2\varphi^{(3)}$) tend to finite non-zero values without inconsistency. At moderate $R_a(k)$, a pseudo-acoustic regime is recovered, which deviates from the pure incompressible ($u_{i,i} = 0$, $p = p_s$) case since the time variation of the $m_{3\alpha}$ term in (28) can be neglected and a WKB approximation can be used to predict the oscillating behaviour of $\hat{d}$ (Sabel'nikov 1975 and DZ). (This oscillating behaviour will be revisited in §5.) For large values of $R_a(k)$, the pressure term in (28) can be neglected compared to the other terms, and the 'pressure released' regime is obtained.

An approach which allows the classification of other relevant limits is available by introducing integrating factors into (28) and (30) so that

$$y = J^{-1}\frac{\hat{\varphi}^{(3)}}{k} \quad \text{and} \quad z = J^{-1}\frac{\hat{p}}{\overline{\rho}a^2} \tag{31}$$

satisfy the simpler equations

$$\frac{\mathscr{D}(\dot{y}/a^2)}{\mathscr{D}t} + k^2 y = \mathrm{i}z^s, \tag{32}$$

$$\frac{\mathscr{D}(\dot{z}/k^2)}{\mathscr{D}t} + a^2 z = a^2 z^s, \tag{33}$$

where $z^s = J^{-1}\hat{p}_s/\overline{\rho}a^2 = \mathrm{i}(J^{-1}/ka^2)m_{3\alpha}\hat{\varphi}^{(\alpha)}$. The left-hand sides of both (32) and (33) are linked only to the dynamics of the solenoidal field and thus decoupled from the dilatational and pressure terms for irrotational mean deformations.

We are now in a position to distinguish the different regimes implied by equations (32) and (33):

(i) The incompressible limit, with $a^2 \to \infty$, which corresponds to a vanishing value of all the time-derivatives in both equations; hence, $\dot{z}^s$ and $y \to 0$, and $z = z^s$ (i.e. $p = p_s$) and $y = 0$ are consistent limits in this case.

(ii) The acoustic regime, recovered when $k^2 y \gg i\dot{z}^s$. By invoking $(\Delta m)^2 \ll 1$ DZ satisfied this condition during their investigation of the acoustic mode.

(iii) A 'pseudo-solenoidal' regime – where the pressure–dilatation correlation is given by the solenoidal pressure variance – which corresponds to $k^2 y = i\dot{z}^s$ in (32) and $z = z^s$ in (33); these equalities hold only if the time-derivative of the solenoidal term (right-hand side of (32)) is much larger than the time-derivative of the dilatational term (first term on the left-hand side of (32)). This regime may be considered to be a subset of the $\Delta m \ll 1$ case.

(iv) The pressure-released limit, corresponding to $k^2 y \ll i\dot{z}^s$ in (32), which leads to the condition

$$\overline{u_{i,i}^2} \ll (\Delta m)^4 \frac{q_s^2}{\ell^2}$$

(with ℓ a lengthscale of the energy-containing turbulence) required for the pressure-released regime to be valid. We mention in passing that if one assumes that the ratio λ of the dilatational to solenoidal kinetic energy is proportional to M_t^2, the above inequality suggests that an alternative to Δm as the parameter that defines the pressure-released regime is the quantity $\Delta m M_t^{-\frac{1}{2}} = r M_t^{\frac{1}{2}}$. In spite of this, the DNS results presented below indicate that the pressure-released limit seems to be adequately parameterized by Δm alone.

For the solenoidal field certain results can be obtained analytically, as is demonstrated below for the case of axial compression, since the solenoidal part of the linear transfer function (see Cambon *et al.* 1992) depends only on the orientation of the wave vector, and not on the modulus; integrations over wave space needed to derive the one-point velocity correlations can thus be separated into the product of two one-dimensional integrals, one of which defines (independently of initial spectra shape) the initial kinetic energy. Evaluation of the non-solenoidal correlations is not as straightforward since the components of the linear transfer matrix that involve the dilatation depend on both the direction $e_i^{(3)} = k_i/k$ of $\boldsymbol{k}$ (as for the solenoidal case) and on its modulus. Accordingly, amplification coefficients in general require numerical integration. This complication is a symptom of the wavenumber dependence of the sonic timescale in spectral space $(a(0)K)^{-1}$, symbolically shown in figure 1(*a*); since the deformation scale D^{-1} is the same for all wavenumbers, above a critical value K^*, the sonic is the shorter of the two timescales. For a given energy spectrum with peak at K_0 so that Δm is characterized by $R_a(K_0)$, the rapid distortion behaviour depends on K/K_0. The largest structures ($K < K_0$) will, therefore, naturally tend toward the pressure-released extreme and the smallest ($K > K_0$) toward the solenoidal limit. When K_0 falls well below K^*, the entire flow is within the pressure-released regime, and $\Delta m \gg 1$; when $K_0 \gg K^*$, the $\Delta m \to 0$ limit is valid (see figure 1*b*).

In the next section, the analysis is applied to the special case of axial compression, and DNS results are used to verify the relevance of Δm as a critical parameter.

3. RDT and DNS of axially compressed flow

Both the RDT and DNS impose upon isotropic compressible turbulence an axial deformation that satisfies the homogeneity condition (15) so that the single non-zero

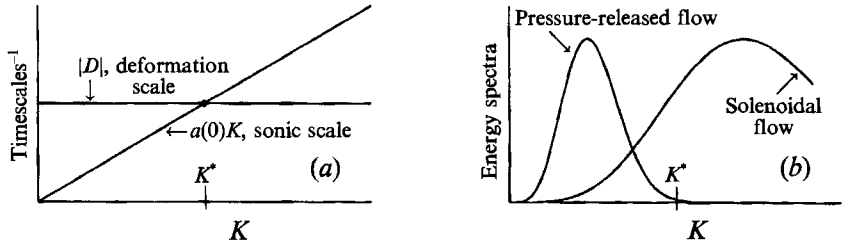

FIGURE 1. Solenoidal and pressure-release regimes: (*a*) timescales; (*b*) energy spectra.

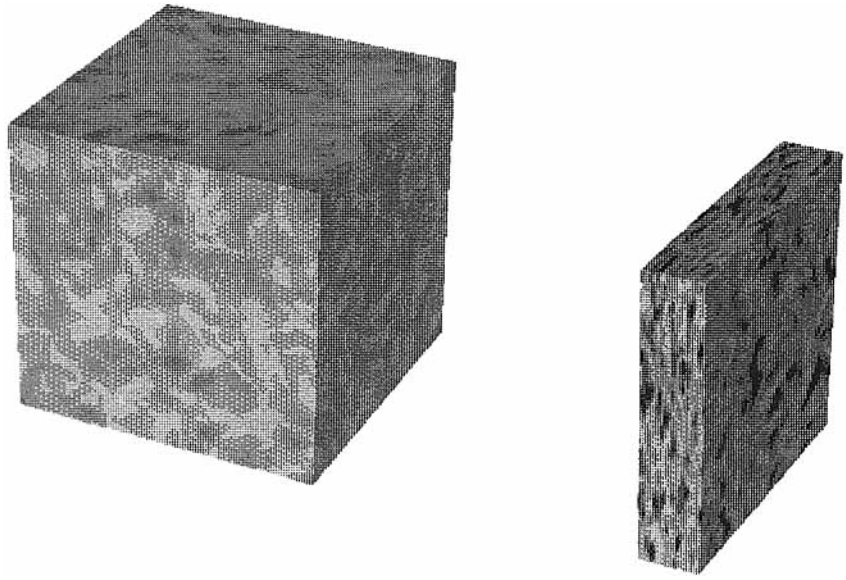

FIGURE 2. Contours of turbulent Mach number (*a*) before and (*b*) after axial compression (Case C).

mean velocity gradient component is

$$U_{1,1} = \frac{D_0}{1 + D_0 t} = D_0 J^{-1} \quad \text{and} \quad F_{11} = J. \tag{34}$$

For $D_0 \equiv D(0) < 0$, this straining can be maintained for a finite time after which the flow volume becomes zero. Here we consider mean density ratios (equal to J^{-1}) that vary from 1 to 5; see figure 2. In the next subsection we specify the RDT correlations relevant to one-point modelling of the axial compression.

3.1. *Rapid distortion analysis for axial compression*

For the case of axial compression, the Craya–Herring–Cambon coordinates given in §2 reduce to $e_1^{(3)} = \cos\theta$ and $e_1^{(2)} = -\sin\theta$, where θ is the angle between $\boldsymbol{k}$ and $\boldsymbol{n}$, and the polar axis is chosen along the compression direction so that $e_1^{(1)} = 0$ (see Cambon & Jacquin 1989 for other axisymmetric RDT applications). The RDT solutions for the solenoidal field are then

$$\widehat{\varphi}^{(1)}(\boldsymbol{k}, t) = J\widehat{\varphi}^{(1)}(\boldsymbol{K}, 0) \quad \text{and} \quad \widehat{\varphi}^{(2)}(\boldsymbol{k}, t) = \frac{K}{k}\widehat{\varphi}^{(2)}(\boldsymbol{K}, 0), \tag{35}$$

with $k_1 = K_1 J^{-1}$, $k_2 = K_2$, $k_3 = K_3$, $\cos\theta = k_1/k = \xi J^{-1}/(1 + C^2\xi^2)^{\frac{1}{2}}$, $k^2 = 1 + C^2\xi^2$, $C^2 = J^{-1} - 1$ and $\xi = K_1/K$. The double correlations are calculated using

$$\widehat{u_i^* u_i} = \widehat{\varphi^{(i)*}\varphi^{(i)}} \quad \text{and} \quad \widehat{u}_1 = -\widehat{\varphi}^{(2)}\sin\theta + \widehat{\varphi}^{(3)}\cos\theta. \tag{36}$$

Assuming isotropic initial data, both the solenoidal and pressure-released analytical RDT predictions can be obtained by integrating either over ξ or directly in physical space, with the results being unaffected by the initial spectral shape. The axial compression correlations are listed below, using as super- or subscripts s and p to denote the solenoidal and pressure-released limiting cases, respectively.

Turbulent kinetic energy:

$$\frac{q_s^2(t)}{q_s^2(0)} = A_s(J), \qquad \frac{q^2(t)}{q^2(0)} = A_p(J). \tag{37a,b}$$

Compression-direction Reynold stress component:

$$\frac{\overline{u_1^s u_1^s}(t)}{q_s^2(0)} = B_s(J), \qquad \frac{\overline{u_1 u_1}(t)}{q^2(0)} = B_p(J). \tag{38a,b}$$

Compression-direction solenoidal–dilatational cross-correlation:

$$\overline{u_1^s u_1^d}(t) = C_s(J) = 0, \qquad \frac{\overline{u_1^s u_1^d}(t)}{q_s^2(0)} = C_p(J). \tag{39a,b}$$

Structure dimensionality tensor, D_{ij} (Reynolds 1992; see also Blaisdell *et al.* 1991 and Cambon 1990):

$$\frac{D_{11}^s(t)}{q_s^2(0)} = D_s(J) = B_s(J), \qquad \frac{D_{11}(t)}{q^2(0)} = D_p(J), \tag{40a,b}$$

where

$$D_{ij}^s \equiv \overline{\psi_{l,i}\psi_{l,j}} = \int 2\frac{k_i k_j}{k^2}\mathscr{E}^s(\boldsymbol{k}, t)\mathrm{d}^3\boldsymbol{k}, \tag{40c}$$

and

$$D_{ij}^d \equiv \overline{\varphi_{,i}\varphi_{,j}} = \int 2\frac{k_i k_j}{k^2}\mathscr{E}^d(\boldsymbol{k}, t)\mathrm{d}^3\boldsymbol{k} \tag{40d}$$

with $\boldsymbol{k} = \boldsymbol{k}(t)$; the second equalities are valid only for the homogeneous case. The vector ψ_i and scalar φ are the result of the Helmholtz decomposition (18), and $\mathscr{E} = \mathscr{E}^s + \mathscr{E}^d$ is the three-dimensional kinetic energy spectrum.

Compression-direction component of the pressure–strain rate correlation, $\Pi_{ij} = \overline{p(u_{i,j} + u_{j,i})}/\bar{\rho}$:

$$\frac{\Pi_{11}^s(t)}{Dq_s^2(0)} = E_s(J), \tag{41a}$$

$$\Pi_{11} = E_p(J) = 0. \tag{41b}$$

The pressure–dilatation term Π is identically zero for both limits.

In terms of the inverse compression ratio J with $C^2 \equiv J^{-2} - 1$, we have for the $J < 1$ case

$$A_s = \frac{1}{2}\left(1 + J^{-2}\frac{\tan^{-1} C}{C}\right), \qquad A_p = \frac{2 + J^{-2}}{3}, \tag{42a,b}$$

$$B_s = \frac{J^{-2}}{2C^2}\left(\frac{1}{2} + \frac{C^2 - 1}{2}\frac{\tan^{-1} C}{C}\right) \qquad B_p = \frac{J^{-2}}{3}, \tag{42c,d}$$

$$C_p = \frac{J^{-2}}{2C^2}\left(-1 + J^{-2}\frac{\tan^{-1} C}{C}\right) - B_s, \tag{42e}$$

$$D_p = \frac{J^{-2}}{C^2}\left(1 - \frac{\tan^{-1} C}{C}\right)\left(\frac{2 + J^{-2}}{3}\right), \tag{42f}$$

$$E_s = \frac{1}{2C^4}\left(C^2 + 3 + (C^2 - 3)J^{-2}\frac{\tan^{-1} C}{C}\right). \tag{42g}$$

The solenoidal amplification functions turn out to be nearly linear in J^{-1}, whereas the pressure-released expressions are nearly parabolic. The quantities A_s and B_s, previously derived by Ribner(1953), and the new expressions D_s and E_s are almost the same as those found for incompressible axisymmetric strain (of arbitrary history), with, for example, the Reynolds stress tensor $R^s_{ij} = \overline{u^s_i u^s_j} = J^{-\frac{2}{3}} R^*_{ij}(J)$, where $\boldsymbol{R}^*$ is the RDT solution for the trace-free part of the mean deformation. Functions A_p and B_p are obtained by simply ignoring the pressure terms during the integration of the equations for the one-point correlations in the rapid axial compression limit, which are

$$\tfrac{1}{2}\dot{q}^2 = -DR_{11} + \Pi, \tag{43}$$

$$\dot{R}_{11} = -2DR_{11} + \Pi_{11}, \tag{44}$$

where $R_{ij} = \overline{u_i u_j}$, and $\Pi = \Pi_{ii}/2 = \overline{pu_{i,i}}/\bar{\rho}$.

For moderate compressibility, we find from the DNS results that the role of Π_{11}, which reduces the anisotropy ($b_{11} = R_{11}/q^2 - \frac{1}{3}$) in (43) and, therefore, *indirectly* reduces the production term in the kinetic energy equation, is more important than the *direct* role of Π. Evidence for this will be presented in the next section, where we use DNS results to test a few aspects of the rapid distortion analysis.

3.2. *Comparison to DNS of rapid axial compression*

The DNS results were obtained using a pseudo-spectral method to solve the compressible Navier–Stokes equations over a homogeneous domain in coordinates that move with the mean deformation (Rogallo 1981; Blaisdell *et al.* 1991; Coleman & Mansour 1991). As mentioned previously, the mean density ratio, $J^{-1} = \bar{\rho}(t)/\bar{\rho}(0)$, varies from 1 to 5 during the compression. The runs use for initial conditions compressible isotropic turbulence at various turbulent Mach numbers that have evolved from velocity fields, with finite dilatational components, that are in near acoustic equilibrium (Sarkar *et al.* 1989); these initial fields are generated by running the code with no mean straining until they develop realistic triple-velocity correlations and dilatational energy for the given M_t. (Note that Blaisdell *et al.* have found that compressible isotropic turbulence strongly depends upon *all* the initial conditions for the dilatational field, not just M_t, which implies that had we begun the precomputation with, for example, a purely solenoidal field, the levels of dilatational energy in the developed flow might be significantly different than those found here.) The initial turbulent Mach number for the runs varies from 0.025 to 0.44, the initial non-dimensional compression speed $r = |D|q^2/\epsilon$ ranges from 47 to 800 (and $|D|/\overline{\omega_i\omega_i}^{\frac{1}{2}}$ from 2 to 88), and the initial values of $\Delta m = M_t|D|q^2/\epsilon$ fall between 1.2 and 178 (while $\Delta m^* \equiv M_t|D|/\overline{\omega_i\omega_i}^{\frac{1}{2}}$ initially lies between 0.26 and 8). A ratio of constant specific heats $\gamma = \frac{5}{3}$ and temperature-dependent viscosity $\mu = T^{0.72}$ are assumed, as is a constant Prandtl number of 0.7. All the runs use 96^3 grid points, and were generated by a version of the code developed by Blaisdell *et al.* (1991) that has been modified to run on the NAS Intel Hypercube/i860 at NASA Ames Research Center.

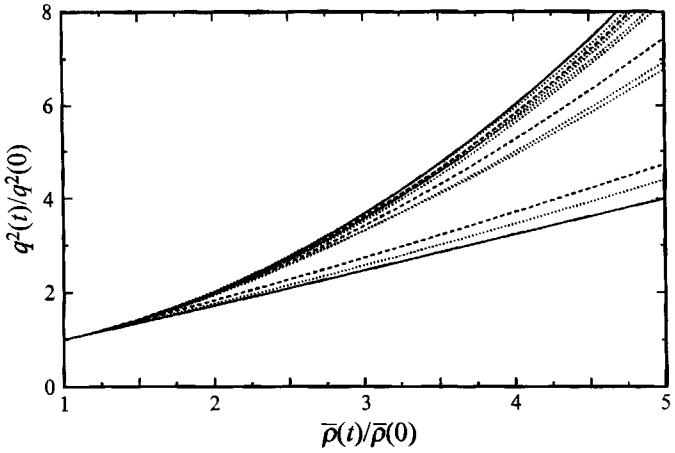

FIGURE 3. Turbulent kinetic energy histories: ——, lower, (37*a*); ——, upper, (37*b*); · · · · ·, DNS with initial Δm ranging from 0.3 (lower) to from 3.0–8.0 (upper); - - - -, DNS results: lower, Case A $(M_t, \Delta m)_{t=0} = (0.025, 5)$; upper, Case B (0.11, 87); middle, Case C (0.29, 29).

Run	$(M_t)_0$	$-(Sq^2/\epsilon)_0$	$(q^4/\epsilon\overline{\nu})_0$	$(\Delta m)_0$	$(\Delta m^*)_0$	$(q_d^2/q^2)_0$	$(\rho_{\rm rms}/\overline{\rho})_0$	$(T_{\rm rms}/\overline{T})_0$
A	0.025	194	358	5	0.3	0.06	0.01	0.005
B	0.11	800	184	87	6.9	0.18	0.05	0.04
C	0.29	100	500	29	1.3	0.09	0.10	0.08

TABLE 1. DNS initial parameters.

Results for the total (solenoidal and dilatational) turbulent kinetic energy will first be presented. In figure 3, the DNS histories for $\overline{\rho u_i u_i}/\overline{\rho}$ are plotted against the mean density ratio $J^{-1} = \overline{\rho}(t)/\overline{\rho}(0)$. (Because it is convenient in the code to solve for momentum rather than velocity, all of the DNS results presented approximate velocity correlations by using density-weighted averages. We find for our purposes that the uncertainty introduced by comparing the DNS Favre averages to the RDT Reynolds averages is unimportant.) These curves strongly support the validity of the RDT analysis presented above, in that all the DNS results lie between the lower solenoidal ('A_s') and upper pressure-released ('A_p') RDT limits – and that the rate of energy amplification scales almost monotonically with the initial value of Δm, which varies from 1.2 for the lower (dotted) curve to from 44 to 178 for the upper (dotted) curves (and with Δm^*, which ranges from 0.3 to from 3 to 8). Three runs will be examined further, those represented by the dashed curves in figure 3. Cases A, B, and C have initial M_t equal to 0.025, 0.11, and 0.29, respectively, but the compression rates are such that the corresponding order for Δm is 5, 87, and 29. The other initial parameters are given in table 1. At the end of the compression the $(M_t, \Delta m)$ values for A, B, and C are respectively (0.03, 18), (0.2, 193), and (0.4, 93). (Note that because the code uses a grid system that deforms with the mean strain (Blaisdell *et al.* 1991) the turbulent fields are resolved throughout the compression, even after the 5-to-1 volume decrease.)

Figure 4 confirms that (37*a*) is an excellent approximation for q_s^2 for the three cases considered and that the solenoidal field is, in fact, unaffected by the dilatational

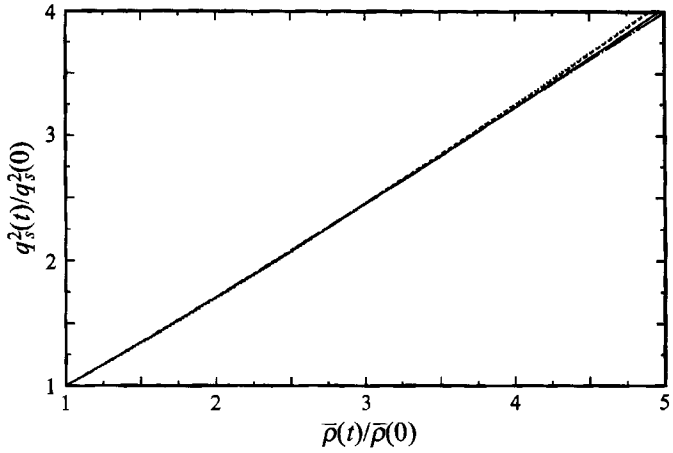

FIGURE 4. Solenoidal turbulent kinetic energy histories: —, Case A; - - - -, Case B; · · · · ·, Case C; —·—, (37*a*).

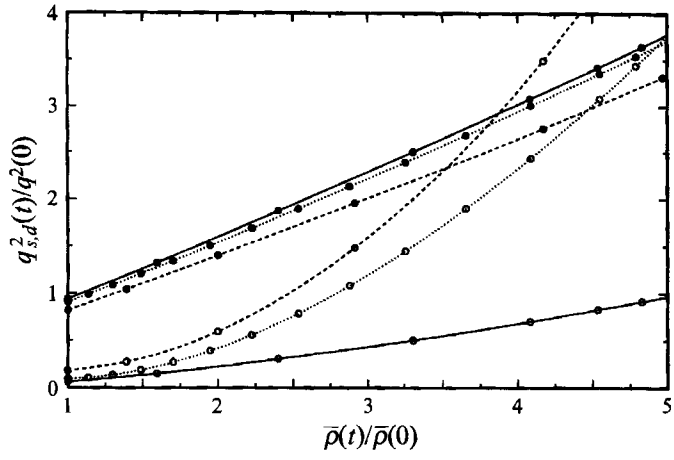

FIGURE 5. Solenoidal and dilatational turbulent kinetic energy histories: •, solenoidal; ○, dilatational; —, Case A; - - - -, Case B; · · · · ·, Case C.

field, as predicted by the RDT. Both contributions to the kinetic energy are shown in figure 5. We see that the dilatational energy is most important at the end of the compression, when the pressure-released regime dominates. The initial values of the dilatational-to-solenoidal energy ratio λ_0 for the various runs is also apparent.

These results suggest the following model for the Mach number dependence of the kinetic energy behaviour during a rapid axial compression:

$$q_s^2(t) = A_s(J) q_s^2(0), \tag{45a}$$

$$q_d^2(t) = A_p(J) q_d^2(0) + \left(A_p^+(J) - A_s^+(J)\right) q_s^2(0), \tag{45b}$$

where the 'interpolation functions' A_p^+ and A_s^+ are assumed to vary monotonically with Δm, increasing from zero to maxima of A_p and A_s, respectively. Similar agreement with DNS data is found for the other correlations given in (42). The results for $\overline{u_1^s u_1^s}$ and $\overline{u_1^d u_1^d}$ are presented on figure 6, where the DNS and RDT histories closely correspond. The slight overamplification of the DNS result compared to the analytical $\overline{u_1^s u_1^s}/q_s^2 = B_s/A_s$

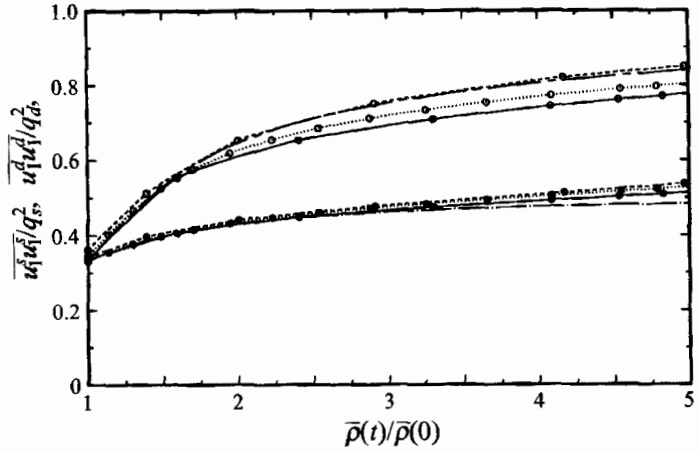

FIGURE 6. Histories of the anisotropy of solenoidal and dilatational turbulent kinetic energy: •, solenoidal; ○, dilatational; —, Case A; - - - -, Case B; · · · · ·, Case C; —·—, (37*a*), (38*a*); — - —, (37*a*, *b*), (38*a*, *b*), using $\lambda_0 = 0.22$ from Case B.

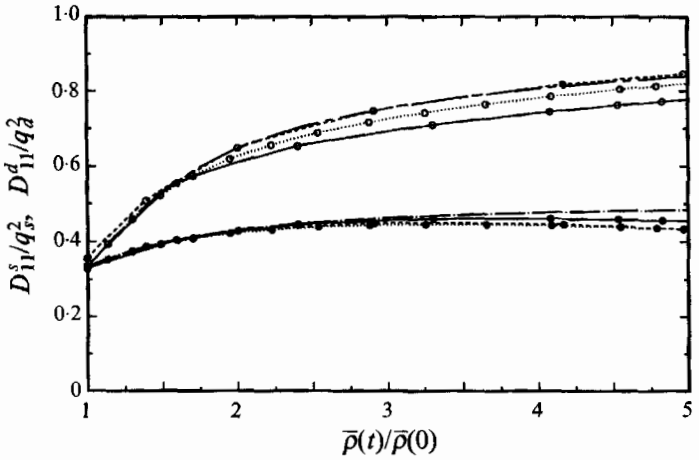

FIGURE 7. Structure tensor histories: •, solenoidal; ○, dilatational; —, Case A; - - - -, Case B; · · · · ·, Case C; —·—, (37*a*), (40*a*); — - —, (37*a*, *b*), (38*a*, *b*), using $\lambda_0 = 0.22$ from Case B.

ratio becomes more pronounced with increasing Δm. For the dilatational curves in figure 6, $\overline{u_1^d u_1^d}/q_d^2$, we find the expected trend with Δm, since they are closest to the analytical pressure-released expression (the 'chain-dash' curve) when Δm is largest. An analogue to (45) is therefore proposed as a model for the dilatational Reynolds stress:

$$\frac{\overline{u_1^d u_1^d}}{q_d^2} = \frac{B_p(J)\lambda_0 + B_p^+(J) - B_s^+(J)}{A_p(J)\lambda_0 + A_p^+(J) - A_s^+(J)}, \tag{46}$$

where the initial dilatational to solenoidal kinetic energy ratio, λ_0, in practice could perhaps be neglected. The curves in figure 6 suggest that the ratio $(B_p^+ - B_s^+)/(B_p - B_s)$ is smaller than the same ratio of 'A' functions.

Another anisotropy measure is presented in figure 7, where the structure tensors are shown. Recall that $D_{11}^d = \overline{u_1^d u_1^d}$. The fact that $D_s = B_s$ in (40*a*) confirms that this

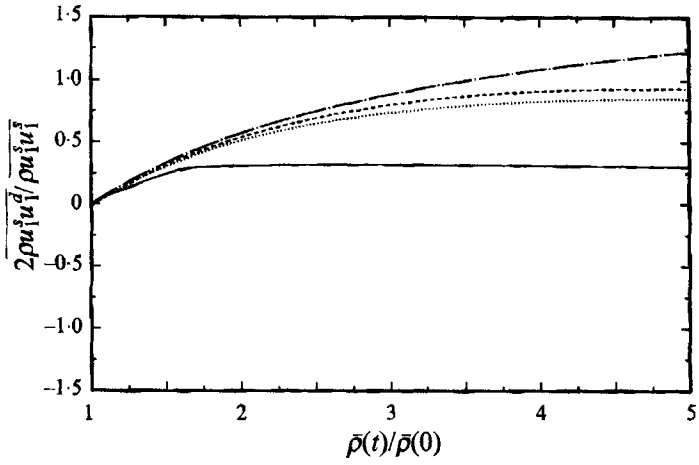

FIGURE 8. Histories of the compression-direction component of the dilatational-solenoidal Reynolds stress correlation: ——, Case A; - - - -, Case B; · · · · ·, Case C; —·—, (38*a*), (39*b*).

equality is a good approximation for axisymmetric strain, as suggested by studies of non-isotropic initial data under rapid rotation (Reynolds 1992; Mansour, Shih & Reynolds 1991). In axisymmetric turbulence, D_{11}/q^2 can be interpreted as an angular coefficient $\cos^2\alpha$, which reveals the conical structure around the symmetry axis of the spectral region that contains energy. For example, a value of $\frac{1}{3}$ for this coefficient suggests no angular dependence (directional isotropy), whereas a value between 0 and $\frac{1}{3}$ suggests a relative concentration of spectral energy in the plane normal to the symmetry axis. Unfortunately, the situation is more complex in the presence of a mean distortion, which causes a variation in direction of the time-dependent wavevector; in the pressure-released case, the angular distribution of spectral energy is unchanged with respect to (isotropic) initial data, but the wavevector tends to be aligned with the symmetry (compression) direction (see (40*c*, *d*)) so that $\cos^2\alpha$ increases and tends to 1. On the other hand, in the pure solenoidal limit, the relative concentration of spectral energy in the plane normal to the compression direction opposes the tendency induced by the wavevector motion so that a slower (as compared to the pressure-released case), but still positive, net increase of the anisotropy is obtained. The solenoidal ratio of D_{11}^s/q_s^2 given by the DNS is found to be slightly lower than the RDT analytical prediction.

The cross-correlation $\overline{u_1^s u_1^d}/\overline{u_1^s u_1^s}$ is plotted in figure 8 and compared to the RDT expression $C_p(J)/B_s(J)$ from (38*a*) and (39*b*). The results suggest that for modelling purposes it might be advantageous to use an effective 'saturated' volumetric ratio J^+ in place of J and define C_p^+, an interpolating function for the cross-correlation, according to

$$\frac{C_p^+(J)}{B_s^+(J)} = \frac{C_p(J^+)}{B_s(J^+)}, \tag{47a}$$

and use the model

$$\overline{u_1^s u_1^d} = C_p(J^+) q_s^2(0). \tag{47b}$$

The parameter J^+ would tend toward the actual J in the pressure-released limit and approach unity in the solenoidal limit. The role of pressure will be discussed further in §4; for now we observe in figures 9 and 10 the dramatic increase of both pressure

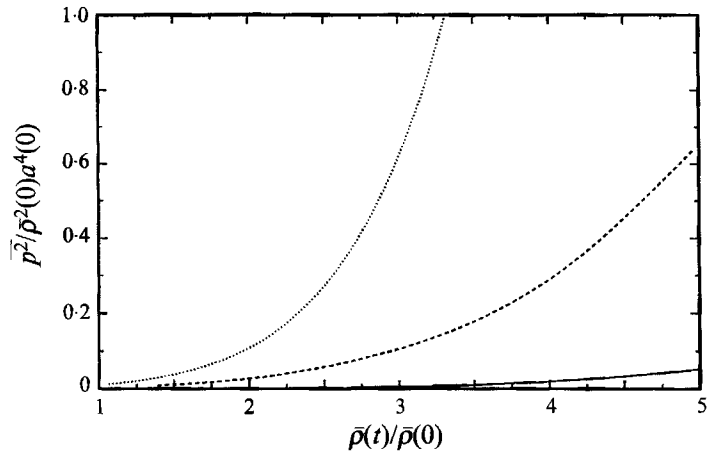

FIGURE 9. Pressure variance histories: ——, Case A; - - - -, Case B; · · · · ·, Case C.

variance and pressure–dilatation terms caused by the compression. The amplification increases with the initial turbulent Mach number, which at first seems to conflict with the idea of a pressure-released limit. The paradox disappears, however, if the pressure–dilatation term is no longer non-dimensionalized by initial values (as is done in figures 9 and 10), but rather scaled by a term proportional to the kinetic energy production. DNS results for Π/Dq^2 are presented on figure 11. The magnitude of this term is found to decrease with increasing Δm for the three cases considered. This implies a non-monotonic variation with Δm for this term (since it is identically zero in the solenoidal limit) with a maximum reached at low compressibility. It can be noticed that increasing values of Π/Dq^2 are found at large J^{-1} for the intermediate Δm case (C), which we expect cannot be explained by RDT. This illustrates that the requirements for a compression to be rapid enough for RDT to be valid are more difficult to meet when the flow is intrinsically compressible, a fact also stressed by Zeman & Coleman (1993). The term Π_{11}/Dq^2 linked to the compression-direction component of the pressure–strain rate correlation is shown in figure 12. The solenoidal RDT expression, $E_s(J)/A_s(J)$, from (37*a*) and (41*a*) is plotted and is found to give an upper limit to the DNS curves. These results suggest a monotonic decrease of Π_{11}/Dq^2 with increasing Δm. Moreover, comparisons of the order of magnitude for both terms in figures 11 and 12 (noting the different scales of the two plots) show that the compression-direction component of the pressure–strain rate is dominant compared to its trace (the pressure–dilatation term) in all cases. This confirms that the reduction of amplification of turbulent kinetic energy with respect to the pressure-released case (where only the 'production' effects are present) is mainly due to Π_{11}, through reduction of anisotropy, as in the pure solenoidal limit.

4. Towards a pressure–strain rate model

Equations for Π_{11} and Π valid for a rapid mean compression can be derived from (43) and (44), using (45) and (46) to model q^2 and $\overline{u_1 u_1}$. The result is

$$\Pi_{11} = J^{-2}\frac{\mathrm{d}}{\mathrm{d}t}(J^2 R_{11}) \tag{48a}$$

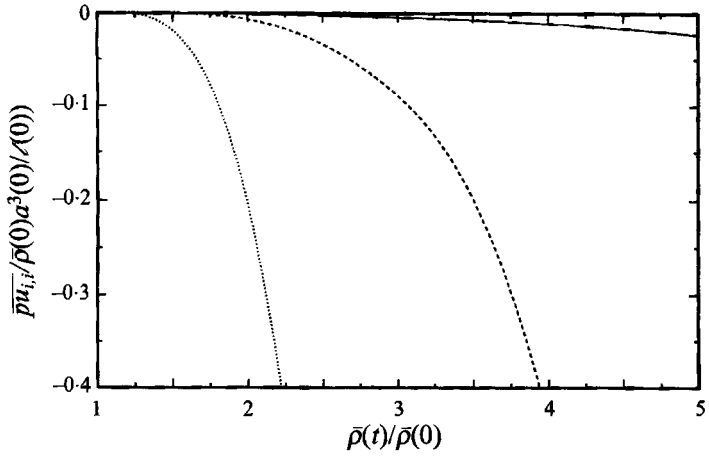

FIGURE 10. Pressure–dilatation correlation histories: symbols as figure 9.

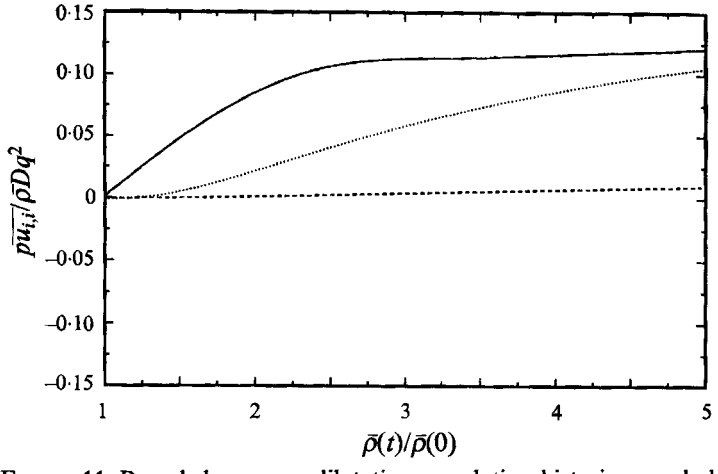

FIGURE 11. Rescaled pressure–dilatation correlation histories: symbols as figure 9.

$$= J^{-2}\frac{\mathrm{d}}{\mathrm{d}t}\left(J^2(B_s + B_p^+ - B_s^+)q_s^2(0) + J^2 B_p q_d^2(0)\right) \tag{48b}$$

$$= DE_s q_s^2(0) + J^{-2}\frac{\mathrm{d}}{\mathrm{d}t}\left(J^2(B_p^+ - B_s^+)\right) q_s^2(0), \tag{48c}$$

and

$$\Pi = \left(\tfrac{1}{2}(\dot{A}_s + \dot{A}_p^+ - \dot{A}_s^+) + D(B_s + B_p^+ - B_s^+)\right) q_s^2(0) \tag{49a}$$

$$= \left(\tfrac{1}{2}(\dot{A}_p^+ - \dot{A}_s^+) + D(B_p^+ - B_s^+)\right) q_s^2(0). \tag{49b}$$

To obtain the above, the relations

$$J^{-2}\frac{\mathrm{d}}{\mathrm{d}t}(J^2 B_s) = E_s;\ \frac{\mathrm{d}}{\mathrm{d}t}(J^2 B_p) = 0;\ \tfrac{1}{2}\dot{A}_s + DB_s = 0;\ \tfrac{1}{2}\dot{A}_p + DB_p = 0, \tag{50}$$

have also been used.

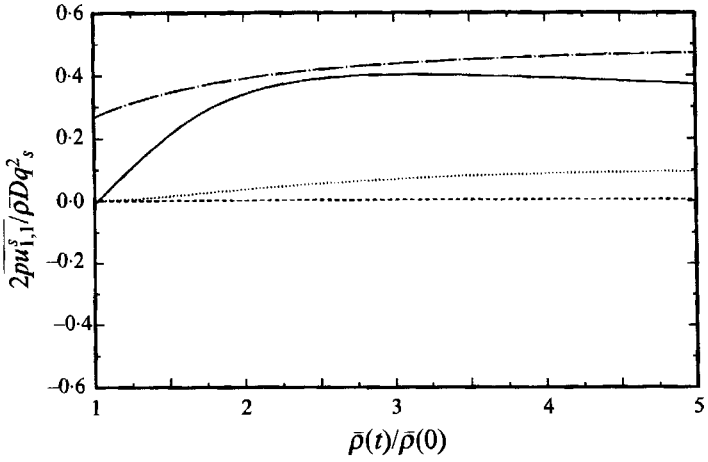

FIGURE 12. Histories of correlation of pressure and compression-direction velocity gradient: —, Case A; - - - -, Case B; · · · · ·, Case C; —·—, (37*a*) and (41*a*).

4.1. *Proposals for second-order modelling*

Two simple ideas for constructing the 'interpolation' functions in (48) and (49) (denoted by a superscript '+') are proposed:

(i) Using two functions of Δm, passing monotonically from from 0 to 1 so that $A_p^+ - A_s^+ = f_1(A_p - A_s)$ and $B_p^+ - B_s^+ = f_2(B_p - B_s)$; if the time-variation of the interpolation functions is neglected, this leads to the model

$$\Pi_{11} = \Pi_{11}^s(1 - f_2), \tag{51a}$$

$$\Pi = (f_2 - f_1)D(B_p - B_s)q_s^2(0). \tag{51b}$$

Note that $f_2 > f_1$ is consistent with the sign of Π found in the DNS results and with the interpretation of dilatational energy histories in figure 5.

(ii) Using a 'saturated' volumetric ratio J^+ instead of the actual J in the evaluation of the interpolation functions, so that $A^+(J) = A(J^+)$. The equation for J^+ would be

$$\dot{J}^+ = U_{i,i}J^+ - (C_{J^+})\frac{a}{\ell}(J^+ - 1), \tag{51c}$$

where C_{J^+} is a modelling constant. The sonic timescale-damping term would allow J^+ to saturate close to unity as the flow regime approaches the solenoidal limit.

4.2. *Testing a second-order model*

Analysis of the three DNS cases shows that they are in the regime where the production and the rapid redistribution terms are dominant. The contribution of the pressure–dilatation is about 10% of the production in the worst case (a value of 15% is found in the DNS data presented by DZ). This leads us in our attempt to model the DNS results to adopt the first proposal of the previous subsection, and consider a linear (in $b_{ij} = \overline{u_i u_j}/q^2 - \delta_{ij}/3$) model for the solenoidal rapid part (see Launder, Reece & Rodi 1975) of the redistribution term, taking $1 - f_2$ in (51*a*) to be an exponential function of Δm. The mean and Reynolds-stress equations then reduce to

$$\bar{\rho}_{,t} = -U_{i,i}\bar{\rho}, \quad U_{i,j} = \frac{D_0}{1 + D_0 t}\delta_{i1}\delta_{j1}, \quad \overline{T}_{,t} = -(\gamma - 1)\overline{T}U_{i,i},$$

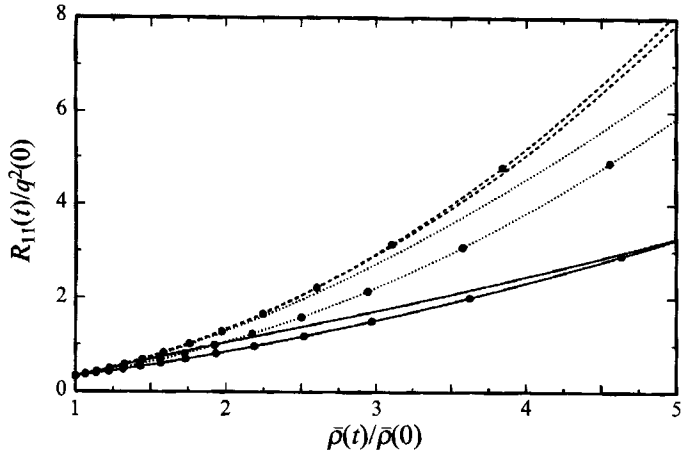

FIGURE 13. Reynolds stress history, compression-direction component: ——, Case A; - - - -, Case B; · · · · ·, Case C; •, (52); no symbols, DNS.

$$R_{ij,t} = -R_{ik}U_{j,k} - R_{jk}U_{i,k} + \Phi_{ij}\exp(-\Delta m/C_{\Delta m}),$$

with

$$\frac{\Phi_{ij}}{\frac{1}{2}q^2} = \tfrac{4}{5}S^*_{ij} + \frac{48\alpha - 60}{35}\left(S^*_{ik}b_{kj} + S^*_{jk}b_{ki} - \tfrac{2}{3}S^*_{mn}b_{mn}\delta_{ij}\right) + \frac{60 - 16\alpha}{15}(\Omega_{ki}b_{kj} + \Omega_{kj}b_{ki}), \quad (52)$$

where $\Delta m = M_t(S_{ij}S_{ji})^{\frac{1}{2}}q^2/\epsilon$ and we have set $\alpha = 2.523$ (to be consistent with the model of Launder *et al.* 1975), and $C_{\Delta m} = 40$. The quantity $\Omega_{ij} = (U_{i,j} - U_{j,i})/2$ is the mean rotation tensor.

The development of the axial component of the Reynolds stress, R_{11}, as predicted by the above model for the three cases considered is shown in figure 13. We find that this simple model, where the effects of the redistributive term diminish when M_t increases, compares well with the DNS data. The development of the turbulent kinetic energy (see figure 14) is also well reproduced, indicating that the effects of the pressure–dilatation are, in fact, weak compared to the production term. No attempt was made to optimize the constant $C_{\Delta m}$ since the pressure–dilatation term was neglected. This term does play a role in the development of the flow, and $C_{\Delta m}$ should be optimized in conjunction with a model for the pressure–dilatation term.

5. Spherical compression and pure shear revisited

5.1. *Isotropic spherical compression*

In the presence of a mean spherical compression, with

$$U_{i,j} = D\delta_{ij}, \quad D = \frac{D_0}{1 + D_0 t} = D_0 J^{-\frac{1}{3}}, \quad F_{ij} = J^{\frac{1}{3}}\delta_{ij} \quad \text{and} \quad k_i = K_i J^{-\frac{1}{3}}, \quad (53)$$

the coupling term $m_{3\alpha}$ in (27) and (28) has zero value. The evolution of the solenoidal kinetic energy is then easily found to be given by the amplification coefficient $J^{-\frac{2}{3}}$. For the dilatational field, (32) and (33) remain of interest now with their right-hand sides equal to zero (since $\hat{p}^s \sim m_{3\alpha}$). Even in the absence of the right-hand sides, a WKB analysis of the equations would not in general be appropriate because the timescale variation of a^2 and k^2 is not necessarily small with respect to the expected frequency

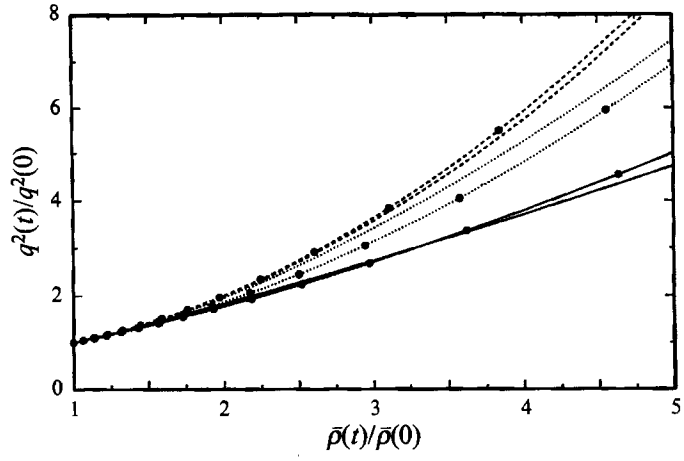

FIGURE 14. Turbulent kinetic energy history: symbols as figure 13.

ak of the oscillating system (depending on the value of Δm). G.A. Blaisdell (1992, private communication) has recently found a solution free of WKB assumptions, valid for arbitrary Δm; the solution is restricted to values of γ close to $\frac{5}{3}$, but a general analytical solution is possible (work in progress). If $\gamma = \frac{5}{3}$, k^2 and a^2 have the same $J^{-\frac{2}{3}}$ time dependence, so simple solutions in terms of $\exp(\pm ia(0)k(t)t)$, where $k(t)$ varies as in (53), can be obtained for y and z. The history of q_d^2 can then be derived from the initial (uncompressed) dilatational field. Assuming that acoustic equilibrium holds for the initial conditions, one can write

$$q_d^2(t) = J^{-\frac{2}{3}} q_d^2(0), \tag{54}$$

which is the same variation found for the solenoidal energy, and corresponds to a pressure-released regime. (The acoustic equilibrium assumption is realistic but perhaps not necessary see Cambon *et al.* 1992.) We thus find that the spherically compressed flow lends support to the general approach advocated in this paper.

5.2. *Pure plane shear*

The case of shear flow is particularly interesting because all the coupling terms, most notably $m_{\alpha 3}$ and $m_{3\alpha}$, are present. The crucial parameter in the absence of compression ($J = 1$) is the shear $S = \mathrm{d}U_1/\mathrm{d}x_2$. Under this deformation, (27) and (32) become

$$\dot{\hat{\varphi}}^{(1)} + S\frac{k_3}{k}\hat{\varphi}^{(2)} = S\left(\frac{k_3 k_2}{(k_1^2 + k_3^2)^{\frac{1}{2}}}\right) y, \tag{55a}$$

$$\frac{\mathscr{D}}{\mathscr{D}t}\left(k\hat{\varphi}^{(2)}\right) = -S\left(\frac{k_1}{(k_1^2 + k_3^2)^{\frac{1}{2}}}\right) k^2 y, \tag{55b}$$

$$\ddot{y} + a_0^2 k^2 y + S^2\frac{k_1^2}{k^2} y = S^2\frac{\mathscr{D}}{\mathscr{D}(St)}\left(\frac{k_1(k_1^2 + k_3^2)^{\frac{1}{2}}}{k^3}\right) k\hat{\varphi}^{(2)}, \tag{56}$$

with

$$U_{i,j} = S\delta_{i1}\delta_{j2},\ k_1 = K_1,\ k_2 = K_2 - K_1 St \quad \text{and} \quad k_3 = K_3.$$

Here the polar axis is chosen to be in the gradient direction ($n_i = \delta_{i2}$). The two solenoidal $\hat{\varphi}^{(1)}$ and $\hat{\varphi}^{(2)}$ components are very close to the set $(\omega_2, \nabla^2 u_2)$ used in linear

stability analyses for decoupling, for example, the Orr–Sommerfeld equations for parallel flows (cf. Waleffe 1990). Even in the pure solenoidal case (where $y = \hat{\varphi}^{(3)}/k = 0$), the present approach appears to be somewhat more tractable than are classic RDT approaches (Townsend 1976). Unlike for a purely irrotational mean deformation, the presence of the new coupling terms (mediated by $m_{13} = -Sk_2k_3/kk_{13}$, $m_{23} = Sk_3/k_{13}$ in the above equations) makes the solenoidal field no longer independent of the dilatational component. In addition, this coupling introduces the new term $S^2(k_1^2/k^2)y$ in (56). The pressure-released approximation amounts to neglecting $a_0^2k^2y$ compared *both* to this new term and to the solenoidal right-hand side in (56). The $\Delta m \gg 1$ regime then implies that (in physical space),

$$u_1 = u_1(0) - Stu_2(0),\ u_2 = u_2(0) \quad \text{and} \quad u_3 = u_3(0),$$

and leads to quadratic amplification, with respect to St, of the kinetic energy (which is more rapid than the nearly linear amplification obtained by numerically integrating over $\boldsymbol{k}$-space the solenoidal RDT solution for $\frac{1}{2}\overline{\hat{\varphi}^{(1)*}\hat{\varphi}^{(1)}} + \frac{1}{2}\overline{\hat{\varphi}^{(2)*}\hat{\varphi}^{(2)}}$). Note that the inviscid *solenoidal* RDT solution for the vertical velocity component is given by $\mathscr{D}(\nabla^2 u_2)/\mathscr{D}t = 0$ in physical space (corresponding to (55) with $y = 0$) so that a rapid decay of u_2 is found. On the other hand, u_2 is conserved in the pressure-released inviscid RDT limit.

6. Recap and conclusions

The objective of this analysis has been to develop a rapid distortion theory for homogeneous compressible turbulence at finite Mach number and then use that theory to explore some issues related to one-point compressible turbulence models. We have applied the analysis to the case of axial compression and found that DNS results confirm the RDT prediction of two distinct flow regimes, one for vanishingly small turbulent Mach number and the other for flows with negligible sonic and turbulent timescale variations compared to the mean distortion. The latter is referred to as the pressure-released regime (since the fluctuating pressure field can be neglected in the RDT for this limit) and is defined by large values of the product of M_t and the ratio of the turbulent to mean deformation timescales. For large values of this parameter, we find that the intrinsic compressibility of the turbulence is responsible for an *increase* in the growth rate of kinetic energy with increasing M_t, an effect exactly opposite to that usually attributed to the compressibility. It would seem that the reduction in kinetic energy growth rate due to compressibility observed in previous compressible homogeneous DNS studies can be attributed to 'slow' terms with nonlinear and dissipative origin, such as the 'extra' dilatational dissipation associated by Zeman (1990) to 'eddy shocklets'.

For the axial compression, analytic expressions for the correlations associated with one-point closures for both the solenoidal and pressure-released limits have been given. These expressions have been used to propose methods of interpolating between the two limiting RDT cases in models for the pressure–strain rate correlation, Π_{ij}, and thus account for finite turbulent Mach number effects.

We are grateful to Professor G. Blaisdell for his contributions to this project. All the DNS results were obtained using the NAS facilities at NASA Ames Research Center. This work is a product of the 1992 Stanford/NASA-Ames Center for Turbulence Research summer program, and was partially supported by the Laboratoire de Mécanique des Fluides et d'Acoustique, Ecole Centrale de Lyon.

REFERENCES

BATCHELOR, G. K. & PROUDMAN, I. 1954 The effect of rapid distortion on a fluid in turbulent motion. *Q. J. Mech. Appl. Maths* **7**, 83.

BLAISDELL, G. A., MANSOUR N. N. & REYNOLDS, W. C. 1991 Numerical simulation of compressible homogeneous turbulence. *Department of Mechanical Engineering, Stanford University, Thermosciences Division Rep.* TF-50.

CAMBON, C. 1982 Etude spectrale d'un champ turbulent incompressible soumis à des effets couplés de déformation et de rotation imposés extérieurement. Thèse d'Etat, Université Claude-Bernard-Lyon I.

CAMBON, C. 1990 Single and double point modeling of homogeneous turbulence. *CTR Annual Research Briefs, Stanford University/NASA Ames.*

CAMBON, C., COLEMAN, G. N. & MANSOUR, N. N. 1992 Rapid distortion analysis and direct simulation of compressible homogeneous turbulence at finite Mach number. In *Proc. 4th Summer Prog., NASA/Stanford Center for Turbulence Research.*

CAMBON, C. & JACQUIN, L. 1989 Spectral approach to non-isotropic turbulence subjected to rotation. *J. Fluid Mech.* **202**, 295.

CAMBON, C., TEISSÈDRE, C. & JEANDEL, D. 1985 Etude d'effets couplés de déformation et de rotation sur une turbulence homogène. *J. Méc. Théor. Appl.* **4**, 629.

COLEMAN, G. N. & MANSOUR, N. N. 1991 Modeling the rapid spherical compression of isotropic turbulence. *Phys. Fluids* A **3**, 2255.

CRAYA, A. 1958 Contribution à l'analyse de la turbulence associée à des vitesses moyennes. *P.S.T. No.* 345.

DEBIÈVE, J. F., GOUIN, H. & GAVIGLIO, J. 1982 Evolution of the Reynolds stress tensor in a shock wave turbulence interaction. *Indian J. Tech.* **20**, 90.

DURBIN, P. A. & ZEMAN, O. 1992 Rapid distortion theory for homogeneous compressed turbulence with application to modelling. *J. Fluid Mech.* **242**, 349 (referred to herein as DZ).

ERINGEN, A. C. 1967 *Mechanics of Continua.* Wiley.

GOLDSTEIN, M. E. 1978 Unsteady vortical and entropic distortions of potential flows round arbitrary obstacles. *J. Fluid Mech.* **89**, 433.

GREENSPAN, H. P. 1968 *The Theory of Rotating Fluids.* Cambridge University Press.

HAYES, W. D. 1957 The vorticity jump across a gasdynamic discontinuity. *J. Fluid Mech.* **2**, 595.

HERRING, J. R. 1974 Approach of axisymmetric turbulence to isotropy. *Phys. Fluids* **17**, 859.

JACQUIN, L., CAMBON, C. & BLIN, E. 1993 Turbulence amplification by a shock wave and rapid distortion theory. Submitted to *Phys. Fluids* A.

LAUNDER, B. E., REECE, G. J. & RODI, W. 1975 Progress in the development of a Reynolds-stress turbulence closure. *J. Fluid Mech.* **68**, 537.

LEE, S., MOIN, P. & LELE, S. K. 1992 Interaction of isotropic turbulence with a shock wave. *Department of Mechanical Engineering, Stanford University, Thermosciences Division Rep.* TF-52.

MANSOUR N. N., SHIH T.-H. & REYNOLDS, W. C. 1991 The effects of rotation on initially anisotropic homogeneous flows. *Phys. Fluids* A **10**, 2421.

REYNOLDS, W. C. 1992 Towards a structure-based turbulence modeling. In *Studies in Turbulence* (ed. T. B. Gatski, *et al.*). Springer.

RIBNER, H. S. 1953 Convection of a pattern of vorticity through a shock wave. *NACA Rep.* 1164.

ROGALLO, R. S. 1981 Numerical experiments in homogeneous turbulence. *NASA TM* 81315.

SABEL'NIKOV, V. A. 1975 Pressure fluctuations generated by uniform distortion of homogeneous turbulence. *Fluid Mech. Soviet Res.* **4**, 46.

SARKAR, S., ERLEBACHER, G., HUSSAINI, Y. M. & KREISS, H. O. 1989 The analysis and modeling of dilatational terms in compressible turbulence. *ICASE Rep.* 89–79.

TOWNSEND, A. A. 1976 *The Structure of Homogeneous Turbulence.* Cambridge University Press.

WALEFFE, F. 1990 On the origin of the streak spacing in turbulent shear flows. *CTR Annual Research Briefs, Stanford, University/NASA Ames.*

WALEFFE, F. 1993 Inertial transfers in the helical decomposition. Submitted to *Phys. Fluids* A.

ZEMAN, O. 1990 Dilatational dissipation: the concept and application in modeling compressible mixing layers. *Phys. Fluids* A **2**, 178.

ZEMAN, O. & COLEMAN, G. N. 1993 Compressible turbulence subjected to shear and rapid compression. *In Turbulent Shear Flows 8* (ed. F. Durst, *et al.*). Springer.